J. Ocean Univ. China (Oceanic and Coastal Sea Research)
https://doi.org/10.1007/s11802-018-3495-9
ISSN 1672-5182, 2018 17 (3): 647-658
http://www.ouc.edu.cn/xbywb/
E-mail:xbywb@ouc.edu.cn

Modeling Monthly Spatial Distribution of *Ommastrephes bartramii* CPUE in the Northwest Pacific and Its Spatially Nonstationary Relationships with the Marine Environment

FENG Yongjiu[1), 2), 3), 4)], LIU Yang[1)], and CHEN Xinjun[1), 3), 4), *]

1) *College of Marine Sciences*, *Shanghai Ocean University*, *Shanghai* 201306, *China*
2) *Function Laboratory for Marine Fisheries Science and Food Production Processes*, *Qingdao National Laboratory for Marine Science and Technology Qingdao* 266235, *China*
3) *Key Laboratory of Sustainable Exploitation of Oceanic Fisheries Resources*, *Shanghai Ocean University*, *Shanghai* 201306, *China*
4) *National Distant-Water Fisheries Engineering Research Center*, *Shanghai Ocean University*, *Shanghai* 201306, *China*

(Received March 21, 2017; revised April 26, 2017; accepted March 6, 2018)

Abstract There are substantial spatial variations in the relationships between catch-per-unit-effort (CPUE) and oceanographic conditions with respect to pelagic species. This study examines the monthly spatiotemporal distribution of CPUE of the neon flying squid, *Ommastrephes bartramii*, in the Northwest Pacific from July to November during 2004–2013, and analyzes the relationships with oceanographic conditions using a generalized additive model (GAM) and geographically weighted regression (GWR) model. The results show that most of the squids were harvested in waters with sea surface temperature (SST) between 7.6 and 24.6℃, chlorophyll-*a* (Chl-*a*) concentration below 1.0 mg m^{-3}, sea surface salinity (SSS) between 32.7 and 34.6, and sea surface height (SSH) between −12.8 and 28.4 cm. The monthly spatial distribution patterns of *O. bartramii* predicted using GAM and GWR models are similar to observed patterns for all months. There are notable variations in the local coefficients of GWR, indicating the presence of spatial non-stationarity in the relationship between *O. bartramii* CPUE and oceanographic conditions. The statistical results show that there were nearly equal positive and negative coefficients for Chl-*a*, more positive than negative coefficients for SST, and more negative than positive coefficients for SSS and SSH. The overall accuracies of the hot spots predicted by GWR exceed 60% (except for October), indicating a good performance of this model and its improvement over GAM. Our study provides a better understanding of the ecological dynamics of *O. bartramii* CPUE and makes it possible to use GWR to study the spatially nonstationary characteristics of other pelagic species.

Key words *Ommastrephes bartramii*; catch-per-unit-effort (CPUE); oceanographic conditions; geographically weighted regression (GWR); spatial nonstationary; Northwest Pacific

1 Introduction

The neon flying squid *Ommastrephes bartramii* inhabits its vast areas of subtropical and temperate waters throughout the world's oceans (Yatsu *et al.*, 2000; Ichii *et al.*, 2004). *O. bartramii* stocks are particularly plentiful in the Northwest Pacific (Chen and Chiu, 2003; Bower and Ichii, 2005; Feng *et al.*, 2017a), and they support the commercial pelagic fisheries of China, Japan, and South Korea (Yan *et al.*, 2009; Yu *et al.*, 2015a). *O. bartramii* is a short-lived, opportunistic species that typically lives for one year (Rodhouse, 2001; Fan *et al.*, 2009) and undergoes extensive seasonal migration between its spawning grounds in subtropical waters and feeding grounds in the Subarctic Boundary and the Transition Domain (Yatsu *et al.*, 1997; Nishikawa *et al.*, 2015). The *O. bartramii* fisheries are highly unstable and respond dynamically and rapidly to changes in the oceanographic environment (Rodhouse, 2001), leading to substantial seasonal, and even monthly, variations in their spatial distribution (Alabia *et al.*, 2015). Knowledge of the squid's spatiotemporal distribution and its relationships with oceanographic conditions are critical to understanding the fishery ecological dynamics and to enable its sustainable exploitation and integrated management.

Spatial distribution is an important, if not essential, feature of fisheries that is of considerable interest to both fishing fleets and scientists (Rodhouse, 2001; Yang *et al.*, 2013; Chen *et al.*, 2016; Feng *et al.*, 2016). Recent pro-

* Corresponding author. E-mail: xjchen@shou.edu.cn

gress in the development of geographical information systems (GIS) and their incorporated spatial analysis tools have facilitated analysis of the spatiotemporal distribution of oceanic species such as *O. bartramii* (Bower and Ichii, 2005; Wang *et al.*, 2010; Meaden and Aguilar-Manjarrez, 2013). In this respect, Hayase (1995) studied the spatial distribution of *O. bartramii* in the North Pacific and identified specific spawning ground boundaries. Ishida *et al.* (1999) examined the summer distribution of *O. bartramii* with respect to the oceanographic structure of the Northwest Pacific from 1992 to 1998. Cao *et al.* (2009) investigated the influence of oceanographic variability on the abundance and distribution of the western winter-spring cohort of *O. bartramii* in the Northwest Pacific. Chen *et al.* (2012) studied the monthly latitudinal centroid of catch-per-unit-effort (CPUE) and analyzed the impact of Kuroshio Current on the spatial distribution of *O. bartramii*. Their results showed that the variation in the strength of Kuroshio Current leads to changes in environmental conditions that can be used to forecast the location of future *O. bartramii* feeding grounds. Recently, Feng *et al.* (2016) identified the spatial hot and cold spots of *O. bartramii* in the Northwest Pacific and revealed their spatial clustering and structure from 2007 to 2010, based on commercial fishery data collected by the Chinese mainland squid-jigging fleets.

La Niña events have been recognized to cause variations in the oceanographic conditions of *O. bartramii* spawning grounds, resulting in decreased squid recruitment, while El Niño events have been found to lead to oceanographic conditions favorable for squid recruitment (Chen *et al.*, 2007; Feng *et al.*, 2017b). A habitat suitability index (HSI) has been used to identify optimal habitats and potential fishing grounds for *O. bartramii* in the Northwest Pacific (Feng *et al.*, 2014). This HSI was developed from the relationship between fishery data from Chinese mainland squid fleets and remotely sensed oceanographic conditions, including sea surface temperature (SST), chlorophyll-*a* (Chl-*a*) concentrations, sea surface salinity (SSS), and sea surface height (SSH). To deduce the relationships between CPUE and oceanographic factors, generalized linear models (GLM) and generalized additive models (GAM) have been applied (Bower and Ichii, 2005; Chen *et al.*, 2008; Yu *et al.*, 2013; Nishikawa *et al.*, 2014). Compared with GLM, GAM can be employed to more robustly explain nonlinear ecological responses to oceanographic conditions (Tian *et al.*, 2010; Drexler and Ainsworth, 2013; Grüss *et al.*, 2014). By integrating longitude and latitude, GAM can evaluate the effect of location on CPUE distribution with spatially stationary coefficients.

However, the relationship between CPUE and oceanographic condition varies across space, and this characteristic is usually described as spatial stationarity (Windle *et al.*, 2009; Tseng *et al.*, 2013). Spatial stationarity cannot be adequately addressed by GLM and GAM; however, geographically weighted regression (GWR) is an effective local modeling technique for spatial analysis that enables the local relationships to be measured and visualized (Fotheringham *et al.*, 1998; Fotheringham *et al.*, 2003). As GWR coefficients are spatially variable, they allow representation of the spatial non-stationarity of *O. bartramii* in the Northwest Pacific.

This paper identifies the monthly spatiotemporal distribution of the *O. bartramii* CPUE in the Northwest Pacific from 2014–2013, and examines its relationship with oceanographic conditions using GAM and GWR. The specific research aims: 1) to analyze the monthly distribution and its variations in responses to oceanographic conditions based on commercial fishery data and remotely sensed environmental data; 2) to examine CPUE-environment relationships using GAM and GWR to identify preferred conditions for *O. bartramii*, where oceanographic factors include SST, Chl-*a*, SSS, and SSH; 3) to evaluate the impact of oceanographic factors on the biological processes and distribution of *O. bartramii*; and 4) to predict spatial patterns of *O. bartramii* using calibrated GAM and GWR models and compare the prediction accuracy and applicability of the two models.

The contribution of this paper is the use of GWR method to address the CPUE-environment relationships of *O. bartramii* that are characterized by spatially varying coefficients. Our research provides a better understanding of the monthly variation of *O. bartramii* CPUE and its relationship with the oceanographic environments, and also illustrates how GWR can be used to represent spatially nonstationary dynamics of other pelagic species.

2 Materials and Methods

2.1 Commercial Fishery Data

Our work focuses on the traditional Northwest Pacific fishing grounds between 148°–161°E and 38°–45°N, from July to November, from 2004 to 2013. Chinese commercial *O. bartramii* fishery records were assembled by the Chinese Squid-jigging Technology Group (CSJTG). These records include fishing dates (year, month, and day), fishing locations (longitude and latitude), the number of vessels in operation each day, and the daily catch of all vessels. Only four fishing companies were involved in squid fishing within the study area during 2004–2007, but the number of vessels has not been accurately reported. In 2009, there were 8 companies and 65 vessels participating in squid fisheries. From 2010 onwards, there were approximately 15 companies involved and 273 vessels were in use; but this number then decreased during 2011–2013. Some vessels reported their daily catch with specific locations and time, while others only reported the total daily catch within a larger spatial grid to ensure the fishing trip was confidential (Yu *et al.*, 2016). These fishery data were aggregated on a monthly basis and applied to a $0.5^\circ \times 0.5^\circ$ spatial grid to reduce the influence of differences between fishing records (Chen *et al.*, 2011). The nominal *CPUE* is expressed as

$$CPUE_{ymij} = \frac{\sum C_{ymij}}{\sum D_{ymij}}, \quad (1)$$

where $CPUE_{ymij}$ is the monthly nominal *CPUE* (t d^{-1}), $\sum C_{ymij}$ is the total catch for all vessels within a fishing grid element, and $\sum D_{ymij}$ is the total fishing days of all vessels within the same fishing grid element at longitude *i* and latitude *j* in month *m* and year *y*.

2.2 Environmental Data

Ocean environmental data were selected using remotely sensed datasets, including Aqua MODIS SST, SeaWiFS MODIS Chl-*a*, Aquarius SSS, and Aquarius SSH. These environmental data cover the same spatial areas and temporal intervals as the *O. bartramii* fishery data mentioned above. Monthly SST and Chl-*a* data yielding a spatial resolution of 4 km were obtained from NASA Ocean Color (oceancolor.gsfc.nasa.gov), monthly SSS data yielding a spatial resolution of $1^\circ \times 1/3^\circ$ were provided by Columbia University (iridl.ldeo.columbia.edu), and monthly SSH data yielding a spatial resolution of $0.25^\circ \times 0.25^\circ$ were provided by NOAA Ocean Watch (oceanwatch.pifsc.noaa.gov). To match the spatial scale of CPUE data, ocean environment data were resampled to a $0.5^\circ \times 0.5^\circ$ grid. Resampling of SST, Chl-*a*, and SSH was accomplished by down-scaling from a finer to coarser scale. Resampling of SSS from $1^\circ \times 0.33^\circ$ to $0.5^\circ \times 0.5^\circ$ was conducted by downscaling from a coarser scale (1°) to a finer scale (0.5°) in the longitude dimension. The downscaling did not improve SSS data precision or quality.

2.3 GAM and GWR Methods

GAM was applied to identify oceanographic (SST, Chl-*a*, SSS, and SSH) and spatiotemporal (location, year, and month) factors affecting the distribution of *O. bartramii* in the Northwest Pacific. GAM is a generalization of a linear regression model that uses unspecified (*i.e.*, nonparametric) smoothing functions in place of linear covariate functions. The method has been shown to be effective in identifying nonlinear relationships between an explained variable and multiple explanatory variables (Hastie and Tibshirani, 1990; Windle *et al.*, 2009; Tseng *et al.*, 2013). The nonparametric GAM for CPUE-environment relationships is

$$\ln(CPUE) \sim s(SST) + s(\mathrm{Chl}a) + s(\mathrm{SSS}) + s(\mathrm{SSH}) + s(\mathrm{Year}) + s(\mathrm{Month}) + s(\mathrm{Longitude}) + s(\mathrm{Latitude}) + \delta, \quad (2)$$

where ln(*CPUE*) is the log-transformed CPUE for *O. bartramii*, *s*(.) are spline smoothing functions, and δ is the model fit residual.

GWR is a set of regression models in which the coefficients are allowed to vary spatially, *i.e.*, the spatial nonstationarity of the datasets accounted for (Brunsdon *et al.*, 1996; Fotheringham *et al.*, 1998; Fotheringham *et al.*, 2003). GWR modeling is also capable of exploring the relationships between a dependent variable and multiple independent variables. The GWR relation in our study is

$$\ln(CPUE) = c_{0(i,j)} + (c_1 \cdot \mathrm{SST}) + (c_2 \cdot \mathrm{Chl}a)_{(i,j)} + (c_3 \cdot \mathrm{SSS})_{(i,j)} + (c_4 \cdot \mathrm{SSH})_{(i,j)} + \varepsilon_{(i,j)} \quad (3)$$

where $c_{0(i,j)}$ is the intercept, c_1 □ $c_{4(i,j)}$ are parameters to be estimated that relate to four oceanographic factors, and $\varepsilon_{(i,j)}$ is the model fitting residual at longitude *i* and latitude *j*.

The GAM model was constructed using R-Gui version 3.2.3 (Wood, 2006; R Development Core Team, 2014) while the GWR model was built using ArcGIS version 10.1. The GAM and GWR models were then used to predict the spatiotemporal distribution of *O. bartramii* in the Northwest Pacific from July to November 2004–2013.

2.4 Evaluation Methods

Several indices were selected to evaluate goodness-of-fit and compare GAM with GWR, including adjusted R^2, Akaike Information Criterion (AIC), mean residual, residual sum of square (RSS), and Moran's I for the residual. An adjusted R^2 value that approaches 1 signifies a good model fit, while smaller AIC values indicate a closer approximation to reality, and hence a more realistic model (Posada and Buckley, 2004; Windle *et al.*, 2009). Smaller values for mean residual and RSS also indicate a better model fit. A well-fit model should yield randomly distributed residuals (Windle *et al.*, 2009). Global Moran's I (Oden and Sokal, 1978) was used to analyze the residuals of GAM and GWR and examine their spatial fit performances. A Moran's I value greater than 0 with $P<0.05$ indicates a positive correlation of residuals that tend to be clustered, whereas a Moran's I value smaller than 0 with $P<0.05$ indicates a negative correlation of residuals that tend to be dispersed. A Moran's I value close or equal to 0 with $P>0.05$ indicates a weak or no autocorrelation and suggests randomly distributed residuals (Mitchell, 2005). Therefore, a well-fit model should yield a Moran's I value close or equal to 0.

Anselin Local Moran's I, a local spatial auto-correlation statistic (Anselin, 1995, 2013) was applied to identify local spatial patterns of CPUE predicted by GAM and GWR. Statistically significant clusters consist of high-high *CPUE* (HH) or low-low *CPUE* (LL), while statistically significant outliers can be a fishing grid element with a high *CPUE* surrounded by fishing grid elements with low *CPUE*s (HL), or a fishing grid element with a low CPUE surrounded by fishing grid elements with high *CPUE*s (LH). The statistically significant clusters of high-high *CPUE* are referred to as hot spots while clusters of low-low *CPUE* are known as cold spots. Based on the results from Anselin Local Moran's I, we computed HH, LL and other categories (including HL, LH, and CPUE being not statistically significant) for both the observed and model-predicted *CPUE*.

An element-by-element method was applied to compare observed and predicted states at the same location. There are four possible results for one element: 1) Hit: both the actual and predicted are HH (or LL); 2) Miss: the actual is HH (or LL) but the predicted is another state; 3) False: the actual is not HH (or LL) but is falsely predicted as HH (or LL); and 4) Correct rejection: both the actual

and predicted are not HH (or LL). These four states correspond to four indicators of accuracy or error (Pontius and Millones, 2011). Two additional indicators, HitOT and overall accuracy, representing the accuracies of models were also used, where the HitOT indicates the percentage of Hit for HH (or LL) considering the total points each month under study. The six indicators were calculated as follows:

$$\begin{cases} \text{HitOT} = \dfrac{\text{Number of HH (or LL) points}}{\text{Total points}} \\ \text{Correct rejection} = \dfrac{\text{Numbers of points being correctly rejected as HH (LL)}}{\text{Total points}} \\ \text{Overall accuracy} = \text{HitOT of HH} + \text{HitOT of LL} + \text{Correct rejection} \\ \text{Hit} = \dfrac{\text{Number of hit HH (or LL) points}}{\text{Observed total HH (or LL) points}} \\ \text{Miss} = \dfrac{\text{Number of missed HH (or LL) points}}{\text{Observed total HH (or LL) points}} \\ \text{False} = \dfrac{\text{Falsely predicted HH (or LL) points}}{\text{Predicted total HH (or LL) points}} \end{cases} . \quad (4)$$

3 Results

3.1 Monthly Distributions of *CPUE* for *O. bartramii*

For the five months from July to November, there were wide differences between the monthly distributions of *CPUE* in fishing locations over the study area within 148˚–161˚E and 38˚–45˚N (Fig.1). The average nominal *CPUE* ranged from 1.48 in July to 2.61 in August, with an increase from July to October followed by a decrease from October to November (Table 1). The highest CPUE ranged from 8.1 in July to 11.8 in August, which was distributed in the area bounded by 155.5˚–157.5˚E and 40.5˚–45˚N. Except for October, the coefficients of variation (CVs) for all months were smaller than 1, indicating low-variances of the *O. bartramii CPUE* in these months. The skewness values were positive in all five months, suggesting left-skewed distributions for *O. bartramii CPUE*. Of the five skewness values, the October value is anomalously large. All Moran's I values were small; however, this does not necessarily indicate a random distribution because high z-scores also suggest some clustering on a local scale. The centroids of the squid fishery for August, September, and October were spatially close in the area bounded by 154.9˚–155.2˚E and 42.3˚–42.9˚N, while the centroids for the remaining two months were located further away (Fig.1 and Table 1).

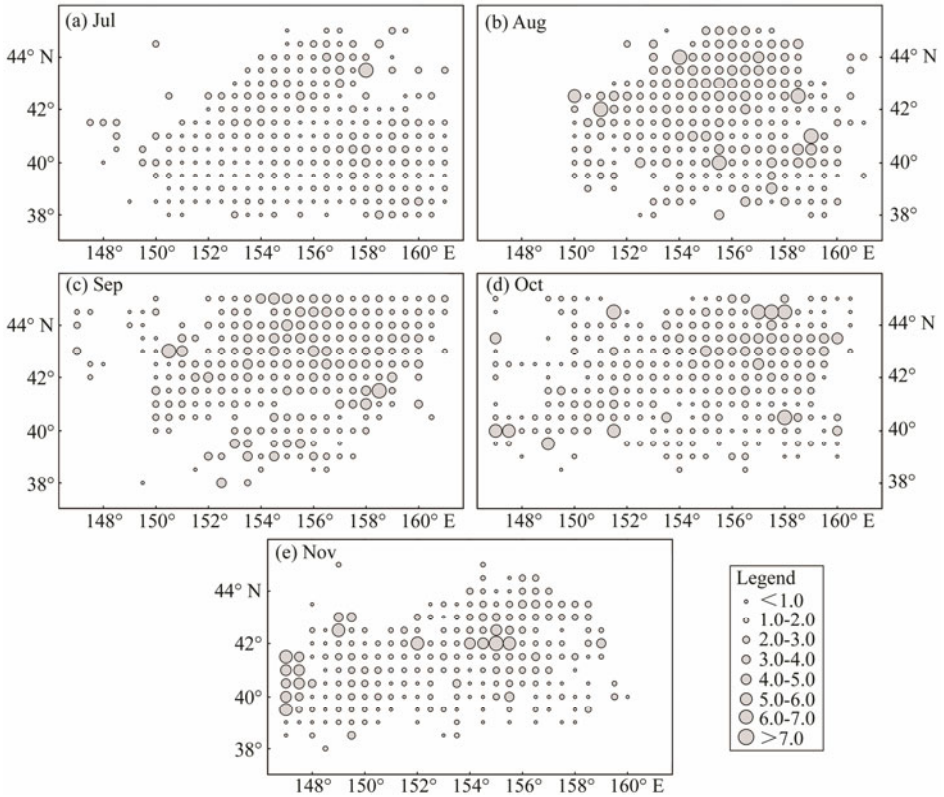

Fig.1 Monthly *CPUE* distributions of *O. bartramii* in Northwest Pacific.

Table 1 Monthly nominal *O. bartramii CPUE* of Chinese squid-jigging fishery in the Northwest Pacific from July to November, averaged over 2004 to 2013

Month	Min	Mean	Max		CV	Skewness	Moran's I		Centroid
			Value	Location			Value	z-score	
7	0.22	1.48	8.1	157.5°E, 40.5°N	0.57	3.77	0.04	11.76	157.5°E, 40.5°N
8	0.14	2.61	11.8	155.5°E, 45.0°N	0.57	2.93	0.05	9.14	155.2°E, 42.3°N
9	0.20	2.58	10.9	156.5°E, 42.5°N	0.52	2.69	0.03	8.32	155.6°E, 42.9°N
10	0.26	2.20	8.5	156.5°E, 43.0°N	1.31	10.15	0.03	5.19	154.9°E, 42.7°N
11	0.10	1.85	8.3	156.5°E, 42.5°N	0.69	1.97	0.02	4.20	153.2°E, 41.8°N

3.2 Monthly Environmental Variations Related to *O. bartramii* Fisheries

Remarkable variations in oceanographic environments were observed in the Northwest Pacific during the main fishing season from July to November (Fig.2). There was a steady increase in average SST from July (17.4℃) to August (19.6℃) and then a continuous decrease from August to November (13.7℃). The average Chl-*a* decreased from 0.3364 mg m^{-3} in July to 0.3112 mg m^{-3} in August, continuously increased from August to October, and then decreased from 0.4798 mg m^{-3} in October to 0.4208 mg m^{-3} in November (Fig.2b). A significant decrease in average SSS from 34.24 in July to 33.34 in September, and an increase from September to November (33.58) were observed. For the average SSH, there was a decrease from 18.89 cm in July to 7.52 cm in September, and then an increase from September to November (15.96 cm).

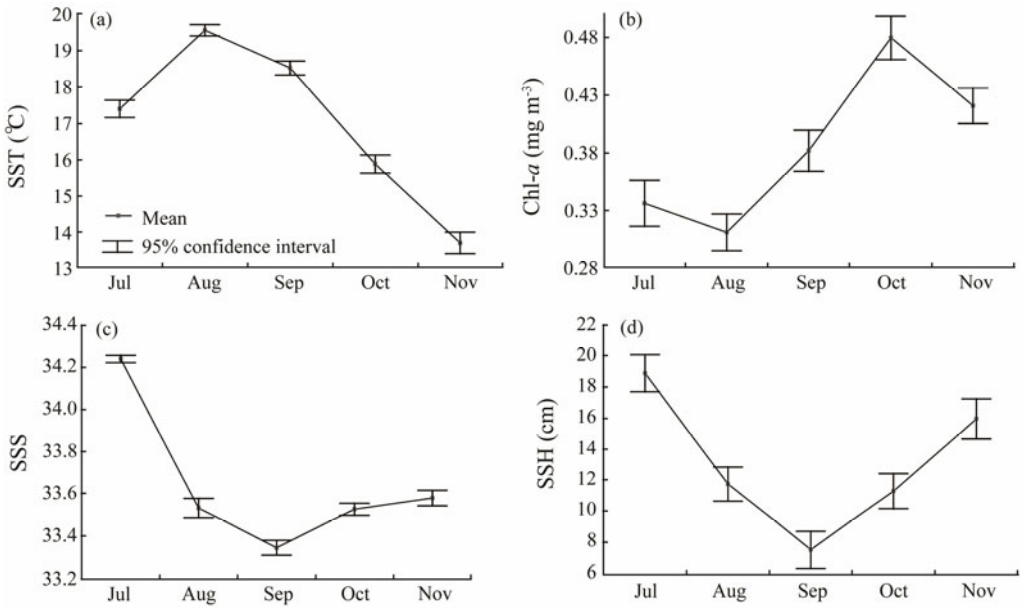

Fig.2 Monthly satellite-derived mean SST, Chl-*a*, SSS, and SSH values related to *O. bartramii* fisheries in the Northwest Pacific, averaged from 2004 to 2013.

3.3 Modeled *CPUE*-Environment Relationships

Each environmental factor was statistically significant in GAM ($P<0.05$), illustrating that all are important in explaining the *CPUE*-environment relationship (Table 2). Total variance explained by the final GAM model was 35.9%, satisfactory for fishery studies. Longitude accounted for the greatest deviance (297.45; 14.4%), followed by SSS (192.43) that accounted for 10.9% and month (86.31) that accounted for 4.2%. Other factors such as SSH, year, and SST explained measurable deviance in the GAM model, whereas Chl-*a* and latitude contributed little to the model and corresponded to the smallest deviances (0.4% and 0.3%, respectively), suggesting weak impacts of the two factors on *O. bartramii CPUE*. The GAM model showed that the distribution of *O. bartramii* significantly varied across longitude and was sensitive to both SSH and month. Thus the three most important variables affecting *O. bartramii CPUE* are longitude, SSS, and month (in descending order of importance).

CPUE increased as SST increased from 5.1 to 22.6℃, and then decreased with the increase of SST (Fig.3a). *O. bartramii* was most abundant in waters with the temperature between 18.1 and 22.6℃. The GAM model suggested a decrease and then an increase of *CPUE* with increasing Chl-*a* (Fig.3b). *CPUE* increased when SSS rose from 31.93 to 33.38 and then decreased with increasing SSS (Fig.3c), and *CPUE* continuously decreased with increasing SSH (Fig.3d). In the spatial domain, greater *CPUE* was noted in waters within 152.5°–158°E and 42°–44°N (Figs.3e–f). Significant inter-annual variability in the distribution of *CPUE* was observed by the Chinese squid-jigging fishery, with greater *CPUE* detected in 2007 and 2011 while smaller *CPUE* detected in

2008 and 2012 (Fig.3g), which confirms the earlier findings of Feng *et al.* (2014). Month by month, greater *CPUE* was observed from August to October, with relatively smaller *CPUE* in July and November (Fig.3h). Overall, most squids were harvested in waters with temperatures between 7.6 and 24.6℃, Chl-*a* below 1.0 mg m^{-3}, SSS between 32.67 and 34.61, and SSH between −12.8 and 28.4 cm.

Table 2 GAM parameter estimates for *O. bartramii* in Northwest Pacific

Variable	Residual deviance	Deviance explained	Percentage of total deviance explained (%)	AIC	Adjusted R^2	*P*
Null	2055.37					
+SST	2018.35	37.02	1.8	7954.73	0.017	<0.05
+Chl-*a*	2010.78	7.57	2.2	7947.66	0.019	<0.01
+SSS	1818.35	192.43	13.1	7605.10	0.045	<0.01
+SSH	1757.61	60.74	14.5	7496.02	0.107	<0.01
+Year	1708.94	48.67	16.9	7408.34	0.123	<0.01
+Month	1622.63	86.31	21.1	7254.91	0.195	<0.01
+Longitude	1325.18	297.45	35.5	6564.47	0.346	<0.01
+Latitude	1318.46	6.72	35.8	6535.84	0.351	<0.01

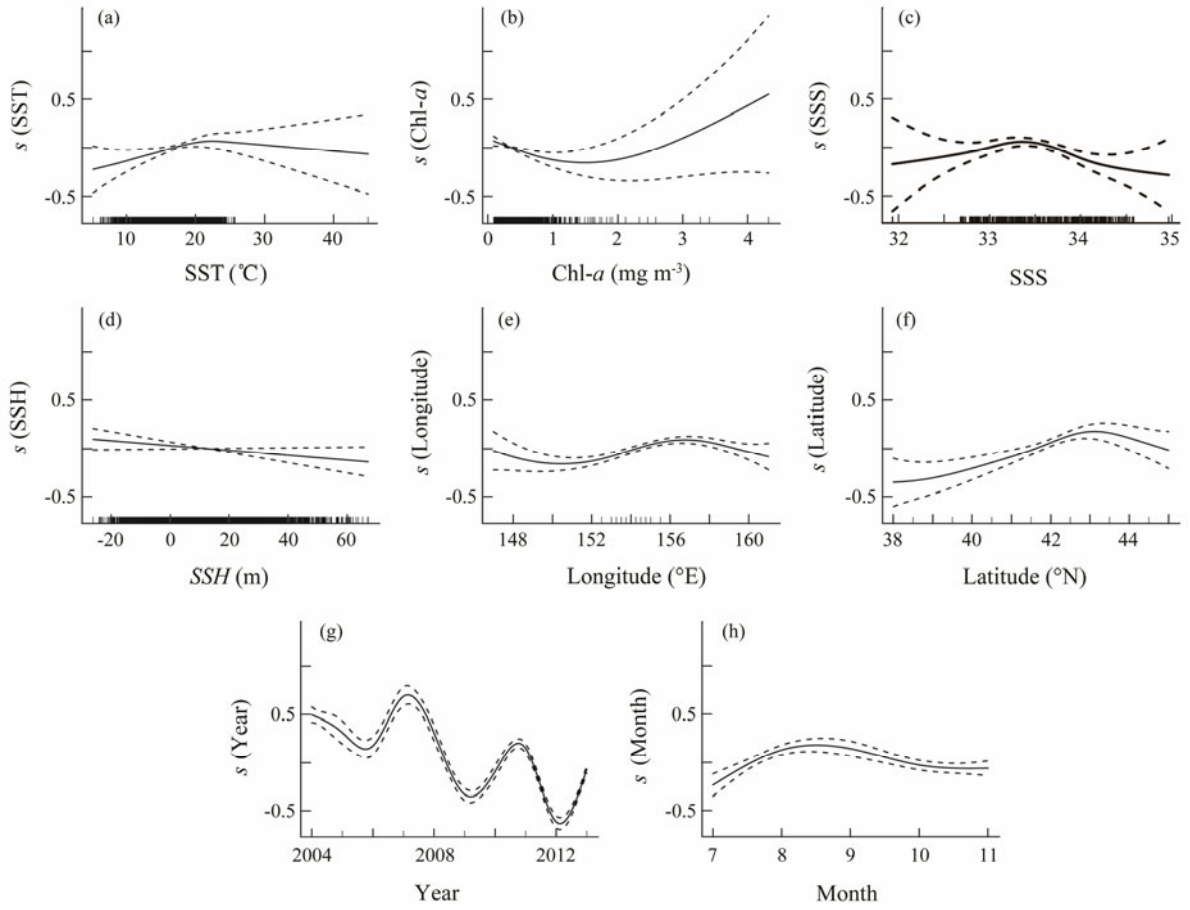

Fig.3 Relationship between *O. bartramii CPUE* and the predicted variables derived from GAM, with 95% confidence intervals (dashed lines).

Table 3 Summary statistics of estimated GWR coefficients with overall percentage of positive and negative values

Variable	Min	Lower quartile	Median	Upper quartile	Max	% −	% +
Intercept	−15.864	−0.885	0.150	0.953	10.320	45.5	54.5
SST	−0.391	−0.002	0.037	0.080	0.748	26.2	73.8
Chl-*a*	−9.781	−0.839	0.009	0.729	9.664	49.3	50.7
SSS	−19.463	−0.974	−0.161	0.389	10.691	56.5	43.5
SSH	−0.793	−0.029	−0.010	0.006	0.559	69.8	30.2

There was a remarkable variation in the local GWR coefficients (Table 3), indicating the presence of spatial non-stationarity in the relationships between the *O. bartramii* CPUE and oceanic environmental factors in the Northwest Pacific. Compared with SST and SSH, the Chl-*a* and SSS coefficients had a range larger than 20,

suggesting stronger spatial variability of these two factors. There were more positive than negative coefficients for SST, while there were more negative than positive coefficients for SSS and SSH. The number of positive and negative coefficients for Chl-*a* were approximately the same. Fig.4 presents a spatial visualization showing the distribution of GWR coefficients at a local scale across the study area.

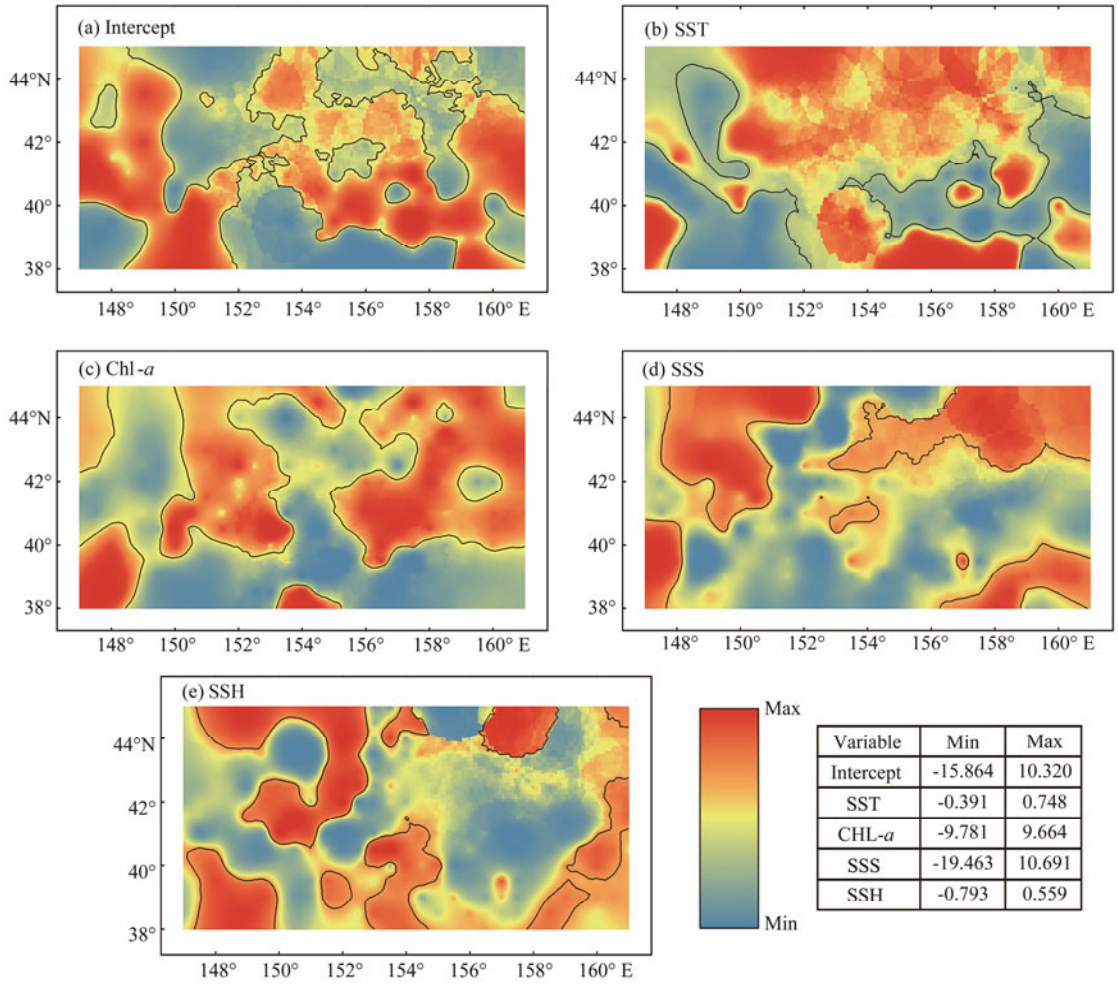

Fig.4 Contoured visualization of estimated GWR coefficients. Thin black lines indicate the zero contour.

4 Discussion

Literature shows that oceanographic conditions in the Northwest Pacific Ocean affect the feeding and growth of neon flying squid, as well as their distribution and migratory patterns (Yu *et al.*, 2015b). Many specific environmental factors have been reported to influence the spawning, growth, and fishing grounds of this species. As a result, the relationships between ocean environmental factors and *O. bartramii CPUE* are complex and are usually spatially variable (*c.f.* Table 3 and Fig.4). Environmental variables such as SST, Chl-*a*, SSS, and SSH are commonly used to model the spatial relationships and patterns of squid (Nishikawa *et al.*, 2015; Feng *et al.*, 2017a; Yu *et al.*, 2016). The results show that about 75.5% of the squid harvested in the study area were from the waters with the following attributes: temperature between 7.6 and 24.6℃, chlorophyll-*a* less than 1.0 mg m^{-3}, salinity between 32.67 and 34.61, and at a height anomaly between −12.8 and 28.4 cm. This result proves that these four factors substantially affected the catch and distribution of *O. bartramii* in the Northwest Pacific during 2004–2013. The selection of these four factors is therefore effective and reasonable in effectively addressing the spatiotemporal changes in catches and *CPUE* of *O. bartramii*.

We suggest that the squid distribution and preferred habitat are dynamic, which can be inferred by GAM and GWR methods. To evaluate and compare the model performances of GAM and GWR, five criteria were selected and then calculated in R-Gui version 3.2.3. GWR included only four oceanographic factors in the model, while GAM used eight. GWR explained the *O. bartramii* CPUE better as measured by five selected criteria (Table 4). The GWR model yielded a higher adjusted R^2 but a lower AIC value, indicating a better fit performance compared to the GAM method. Both models had mean residuals approaching zero, while the residual sum of squares (RSS) for GWR was smaller by 178.79, confirming its superior performance. As shown by Moran's I and its *P*-value, the residuals from both models yielded random distributions; however, that of GWR was stronger

because of its higher *P*-value. Although locations for oceanographic factors were not explicitly included in GWR, they were substantially considered when using this method to explain spatial non-stationarity. The fishing year and month were not included in GWR modeling because they complicated the model and did not improve its adjusted R^2 and AIC.

The monthly spatial distributions of *O. bartramii* predicted by the GAM and GWR models were quite similar, and they are also similar to the observed nominal *CPUE* patterns averaged over 2004–2013 (*c.f.* Fig.1 and Fig.5). Of the summary statistics for monthly *CPUE*, the predicted average *CPUE* was greater than that of the observed, but the largest *CPUE* was smaller, suggesting more evenly distributed *CPUE* than predicted by the models (Table 5). The highest *CPUE* predicted by GAM ranges from 3.2 in July to 5.8 in August in an area bounded by 154.5˚–156.5˚E and 40.5˚–43.5˚N. The highest *CPUE* predicted by GWR ranges from 5.5 in July to 9.7 in August, which was distributed in the area bounded by 153.5˚–158.5˚E and 40.5˚–44.5˚N. The CVs inferred from the models are smaller than the observed results for all months, suggesting low-variances of the predicted *CPUE*. Both the observed and predicted *CPUE* distribu-

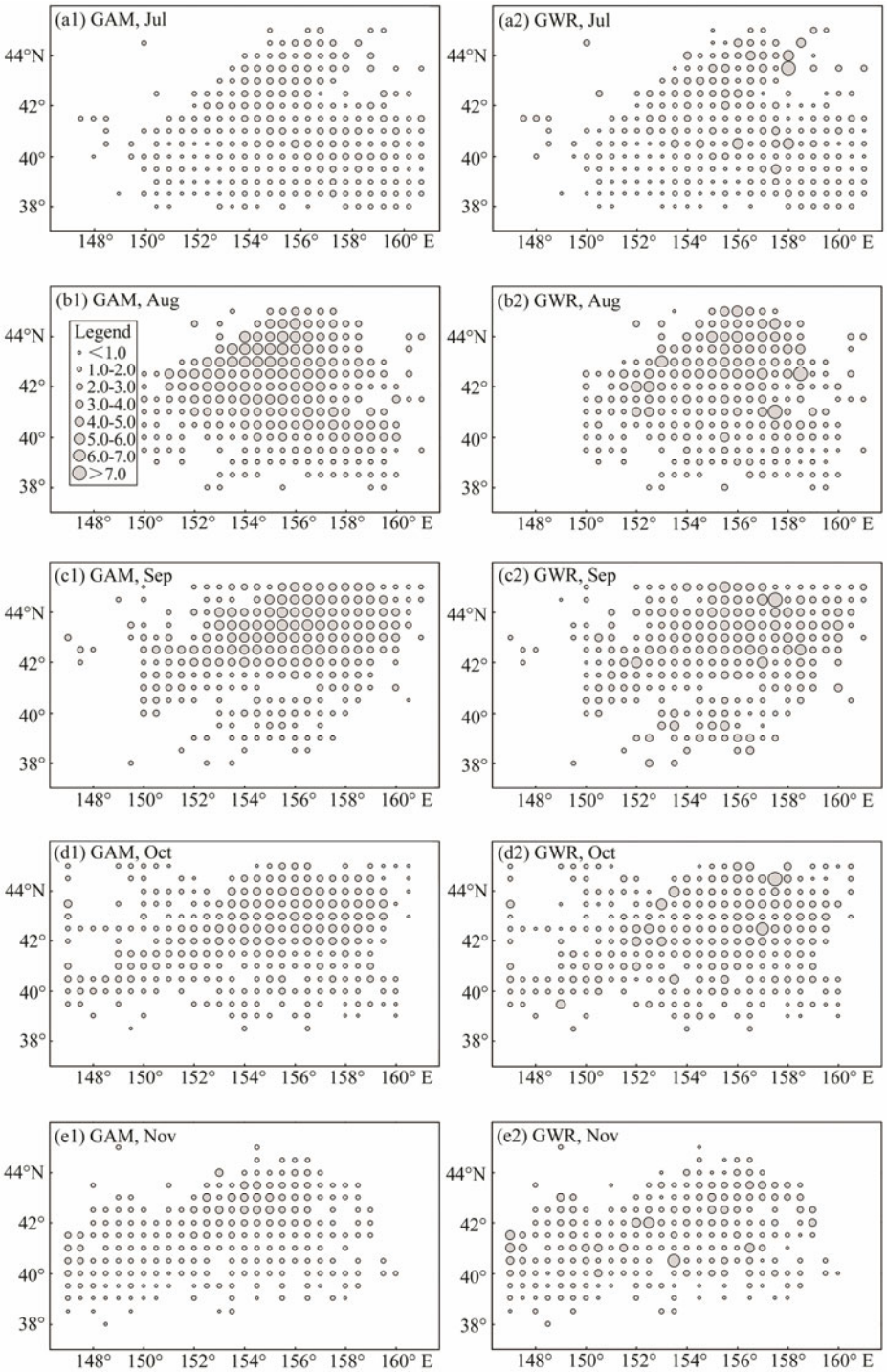

Fig.5 Comparison of the predicted *O. bartramii* CPUE modeled by GAM and GWR.

Table 4 Comparison of goodness-of-fit for GAM and GWR models used to infer *CPUE*-environment relationships for *O. bartramii* in the Northwest Pacific

Model	Adjusted R^2	AIC	Residual			
			Mean	Sum of squares	Moran's I	*P*-value
GAM	0.351	6547.01	−0.000086	1323.19	0.0098	0.06
GWR	0.379	5197.99	0.000009	1144.40	−0.0044	0.32

Table 5 July–November statistics of *O. bartramii CPUE* predicted by GAM and GWR models

Model	Month	Min	Mean	Max		CV	Skewness	Moran's I		Centroid
				Value	Location			Value	z-score	
GAM	7	0.42	1.58	3.2	156.0°E, 40.5°N	0.36	0.13	0.46	35.85	155.7°E, 41.2°N
	8	1.15	2.95	5.8	155.5°E, 43.5°N	0.40	0.41	0.72	25.00	155.5°E, 41.8°N
	9	0.94	2.73	5.4	156.5°E, 43.5°N	0.39	0.57	0.59	42.35	155.2°E, 42.6°N
	10	0.79	2.09	4.3	156.0°E, 43.0°N	0.41	0.62	0.76	27.29	154.5°E, 42.2°N
	11	0.77	1.68	3.8	154.5°E, 43.5°N	0.39	1.27	0.52	32.36	153.3°E, 41.6°N
GWR	7	0.42	1.70	5.5	158.0°E, 43.5°N	0.59	2.81	0.22	17.81	155.8°E, 41.3°N
	8	0.21	2.61	9.7	158.5°E, 42.5°N	0.64	5.30	0.21	8.24	155.5°E, 41.9°N
	9	0.35	2.65	7.3	157.5°E, 44.5°N	0.39	0.81	0.26	18.82	155.3°E, 42.3°N
	10	0.57	2.09	6.3	157.5°E, 44.5°N	0.56	4.69	0.29	11.44	154.5°E, 42.2°N
	11	0.45	1.81	6.5	153.5°E, 40.5°N	0.49	1.64	0.05	3.22	153.1°E, 41.5°N

tions are left-skewed. In all months, predicted *CPUE* is highly clustered as demonstrated by the high Moran's Indices and their z-scores. The centroids predicted by GAM are located in the area bounded by 153.3°–155.7°E and 41.2°–42.6°N, while those predicted by GWR are bounded by 153.1°–155.8°E and 41.3°–42.3°N (Table 5). The two models produced similar results. Overall, the *CPUE* distribution results modeled by GWR more closely agreed with the observed values.

The monthly spatial distributions of *O. bartramii* predicted by the GAM and GWR models were quite similar, and they are also similar to the observed nominal *CPUE* patterns averaged over 2004–2013 (*c.f.* Fig.1 and Fig.5). Of the summary statistics for monthly *CPUE*, the predicted average *CPUE* was greater than that of the observed, but the largest *CPUE* was smaller, suggesting more evenly distributed *CPUE* than predicted by the models (Table 5). The highest *CPUE* predicted by GAM ranges from 3.2 in July to 5.8 in August in an area bounded by 154.5°–156.5°E and 40.5°–43.5°N. The highest *CPUE* predicted by GWR ranges from 5.5 in July to 9.7 in August, which was distributed in the area bounded by 153.5°–158.5°E and 40.5°–44.5°N. The CVs inferred from the models are smaller than the observed results for all months, suggesting low-variances of the predicted *CPUE*. Both the observed and predicted *CPUE* distributions are left-skewed. In all months, predicted *CPUE* is highly clustered as demonstrated by the high Moran's Indices and their z-scores. The centroids predicted by GAM are located in the area bounded by 153.3°–155.7°E and 41.2°–42.6°N, while those predicted by GWR are bounded by 153.1°–155.8°E and 41.3°–42.3°N (Table 5). The two models produced similar results. Overall, the *CPUE* distribution results modeled by GWR more closely agreed with the observed values.

The hot and cold spots of observed and predicted *CPUE* were computed using Anselin Local Moran's I using ArcGIS (Anselin, 1995; Anselin *et al.*, 2006). An overlay map comparing the observed and predicted hot/cold spots was created for each month (Fig.6). Visual inspection shows a general similarity between the overall patterns produced by the GAM and GWR models for all months, but significant differences are detected on local scales (Table 6). The July hot spots are located in the northeastern part of the study area bounded by 155°–160°E and 39°–40.5°N, while the cold spots are located in the southwestern part bounded by 149.5°–152°E and 38°–41°N. Later in August, the hot spots move westward by about 2° and all are located to the north of 41.5°N, while the cold spots in August move to the south of 40°N. In September, the hot spots are in similar locations to those in August, while the cold spots move back to where they were in July in the southwestern part. The cold spots in October reduced in size compared to those in the previous three months, and hot spots in November are also significantly smaller than those in the previous four months, thereby suggesting less clustering which is also confirmed by the small Moran's I and z-scores (Table 1).

The overall accuracies of determining hot spots in July and August exceed 60% for GAM, but those in the other three months are less than 60% (Table 6). Except for October, the overall accuracy for GWR exceeds 60%, indicating the solid performance of this model. The overall accuracy of GAM in July is greater than that of GWR while those in August are similar. The remaining three months show that GWR is more accurate than GAM. For both models, the accuracy in July and August is mainly due to the correct prediction of hot and cold spots, while the accuracy in September and October is mainly attributed to the correct prediction of hot spots and other statistically non-significant categories. The accurate GWR predictions in November are largely related to other statistically non-significant categories (42.3%), while the hot spots, cold spots, and other statistically non-significant categories make a similar contribution to the GAM model for November.

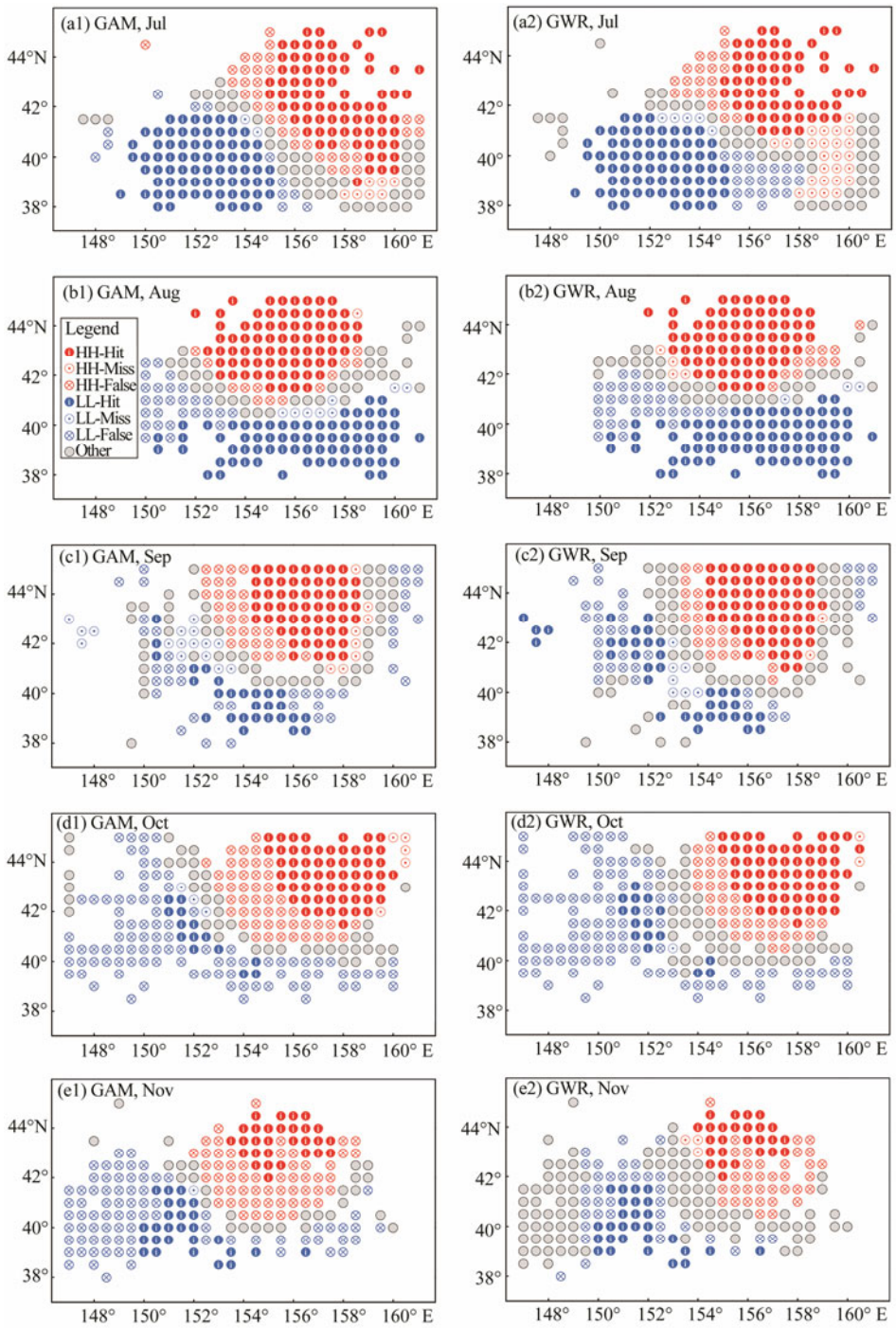

Fig.6 Comparison of the predicted hot spots of *O. bartramii CPUE* from GAM and GWR models.

Table 6 Comparison of prediction accuracies (%) between GAM and GWR models

Model	Month	Overall accuracy	HitOT		Correct due to other	HH-Hot spot			LL-Cold spot		
			HH	LL		Hit	Miss	False	Hit	Miss	False
GAM	7	78.3	31.0	29.1	18.2	92.0	8.0	30.4	97.4	2.6	13.8
	8	79.0	32.2	30.9	15.9	98.7	1.3	14.8	90.0	10.0	27.3
	9	58.8	25.3	11.6	21.9	88.1	11.9	33.7	62.8	37.2	60.9
	10	43.7	22.6	5.3	15.8	92.3	7.7	43.9	82.4	17.6	87.2
	11	38.7	13.2	12.3	13.2	100.0	0.0	65.9	96.4	3.6	74.3
GWR	7	71.7	24.0	27.9	19.8	71.3	28.7	25.3	93.5	6.5	23.4
	8	79.0	30.9	33.0	15.1	94.7	5.3	13.3	96.3	3.8	28.7
	9	71.3	27.9	15.5	27.9	97.0	3.0	25.3	83.7	16.3	50.0
	10	47.4	23.7	6.0	17.7	96.9	3.1	36.4	94.1	5.9	86.3
	11	66.8	11.8	12.7	42.3	89.7	10.3	57.4	100.0	0.0	55.6

5 Conclusions

We examined the monthly distributions and the *CPUE*-environment relationships of *O. bartramii* in the traditional Chinese squid-jigging fishing grounds in the Northwest Pacific from July to November, between 2004 and 2013. The results indicate that the observed average nominal *CPUE* ranges from 1.48 in July to 2.61 in August, increasing from July to October and decreasing from October to November. The highest CPUE values range from 8.1 in July to 11.8 in August and are distributed in an area bounded by 155.5°–157.5°E and 40.5°–45°N. Our results also show that most of the squids (about 75.5%) were harvested in waters with SST between 7.6 and 24.6℃, Chl-*a* less than 1.0 mg m^{-3}, SSS between 32.67 and 34.61, and SSH between −12.8 and 28.4 cm.

The *CPUE*-environment relationships for *O. bartramii* were examined using GAM and GWR modeling, and the spatial patterns of CPUE were predicted from July to November using calibrated models. The GWR method showed notable variation in local coefficients, indicating the presence of spatial non-stationarity in the relationships between the *O. bartramii CPUE* and the oceanographic conditions. In addition, there were nearly equal positive and negative coefficients for Chl-*a*, more positive than negative coefficients for SST, and more negative than positive coefficients for SSS and SSH. The overall hot spot accuracy in July and August exceeded 60% for GAM, but the accuracies for September, October, and November were less than 60%. Excluding October, the overall accuracies for GWR exceeded 60%, indicating good performance of this model. In comparison, GAM is better at identifying the preferred conditions for *O. bartramii,* while GWR is more effective in capturing the spatial non-stationarity in ecological dynamics. Our results contribute to a better understanding of the spatiotemporal distributions of *CPUE* and the impact of oceanographic variables on the *O. bartramii* fisheries in the Northwest Pacific.

Acknowledgements

This study was financially supported by the National Natural Science Foundation of China (No. 41406146) and Function Laboratory for Marine Fisheries Science and Food Production Processes, Qingdao National Laboratory for Marine Science and Technology, China (No. 2017-1A02).

References

Alabia, I. D., Saitoh, S. I., Mugo, R., Igarashi, H., Ishikawa, Y., Usui, N., Kamachi, M., Awaji, T., and Seito, M., 2015. Seasonal potential fishing ground prediction of neon flying squid (*Ommastrephes bartramii*) in the western and central North Pacific. *Fisheries Oceanography*, **24** (2): 190-203.

Anselin, L., 1995. Local indicators of spatial association-LISA. *Geographical Analysis*, **27** (2): 93-115.

Anselin, L., 2013. *Spatial Econometrics: Methods and Models*. Springer Science & Business Media, Heidelberg, 13-15.

Anselin, L., Syabri, I., and Kho, Y., 2006. GeoDa: An introduction to spatial data analysis. *Geographical Analysis*, **38** (1): 5-22.

Bower, J. R., and Ichii, T., 2005. The red flying squid (*Ommastrephes bartramii*): A review of recent research and the fishery in Japan. *Fisheries Research*, **76** (1): 39-55.

Brunsdon, C., Fotheringham, A. S., and Charlton, M. E., 1996. Geographically weighted regression: A method for exploring spatial nonstationarity. *Geographical Analysis*, **28** (4): 281-298.

Cao, J., Chen, X., and Chen, Y., 2009. Influence of surface oceanographic variability on abundance of the western winter-spring cohort of neon flying squid *Ommastrephes bartramii* in the NW Pacific Ocean. *Marine Ecology-Progress Series*, **381**: 119.

Chen, C.-S., and Chiu, T.-S., 2003. Variations of life history parameters in two geographical groups of the neon flying squid, *Ommastrephes bartramii*, from the North Pacific. *Fisheries Research*, **63** (3): 349-366.

Chen, X., Cao, J., Chen, Y., Liu, B., and Tian, S., 2012. Effect of the Kuroshio on the spatial distribution of the red flying squid *Ommastrephes Bartramii* in the Northwest Pacific Ocean. *Bulletin of Marine Science*, **88** (1): 63-71.

Chen, X., Liu, B., and Chen, Y., 2008. A review of the development of Chinese distant-water squid jigging fisheries. *Fisheries Research*, **89** (3): 211-221.

Chen, X., Tian, S., Chen, Y., Cao, J., Ma, J., Li, S., and Liu, B., 2011. *Fishery Biology for Ommastrephes bartramii in the Northwestern Pacific Ocean*. Science Press, Beijing, 306pp.

Chen, X., Zhao, X., Chen, Y., 2007. Influence of El Niño/La Niña on the western winter–spring cohort of neon flying squid (*Ommastrephes bartramii*) in the northwestern Pacific Ocean. *ICES Journal of Marine Science*, **64** (6): 1152-1160.

Chen, Y., Shan, X., Jin, X., Yang, T., Dai, F., and Yang, D., 2016, A comparative study of spatial interpolation methods for determining fishery resources density in the Yellow Sea. *Acta Oceanologica Sinica*, **35** (12): 65-72.

Drexler, M., and Ainsworth, C. H., 2013. Generalized additive models used to predict species abundance in the Gulf of Mexico: An ecosystem modeling tool. *PLoS One*, **8** (5): e64458.

Fan, W., Wu, Y., and Cui, X., 2009. The study on fishing ground of neon flying squid, *Ommastrephes bartrami*, and ocean environment based on remote sensing data in the Northwest Pacific Ocean. *Chinese Journal of Oceanology and Limnology*, **27**: 408-414.

Feng, Y., Chen, X., Yang, X., and Gao, F., 2014. HSI modeling and intelligent optimization for fishing ground forecast by using genetic algorithm. *Acta Ecologica Sinica*, **34** (15): 4333-4346.

Feng, Y., Chen, X., and Liu, Y., 2016. The effects of changing spatial scales on spatial patterns of CPUE for *Ommastrephes bartramii* in the northwest Pacific Ocean. *Fisheries Research*, **183**: 1-12.

Feng, Y., Chen, X., and Liu, Y., 2017a. Detection of spatial hot spots and variation for the neon flying squid (*Ommastrephes bartramii*) resources in the Northwest Pacific Ocean. *Chinese Journal of Oceanology and Limnology*, **35** (4): 921-935.

Feng, Y., Cui, L., Chen, X., and Liu, Y., 2017b. A comparative study of spatially clustered distribution of jumbo flying squid (*Dosidicus gigas*) offshore Peru. *Journal of Ocean University of China*, **16** (3): 1-11.

Fotheringham, A. S., Brunsdon, C., and Charlton, M., 2003.

Geographically Weighted Regression. John Wiley & Sons, Limited, West Atrium, 159-183.

Fotheringham, A. S., Charlton, M. E., and Brunsdon, C., 1998. Geographically weighted regression: A natural evolution of the expansion method for spatial data analysis. *Environment and Planning A*, **30** (11): 1905-1927.

Grüss, A., Drexler, M., and Ainsworth, C. H., 2014. Using delta generalized additive models to produce distribution maps for spatially explicit ecosystem models. *Fisheries Research*, **159**: 11-24.

Hastie, T. J., and Tibshirani, R. J., 1990. *Generalized Additive Models*. CRC Press, Boca Raton, 136-166.

Hayase, S., 1995. Distribution of spawning grounds of flying squid, *Ommastrephes bartrami*, in the North Pacific Ocean. *Japan Agricultural Research Quarterly*, **29**: 65-65.

Ichii, T., Mahapatra, K., Sakai, M., Inagake, D., and Okada, Y., 2004. Differing body size between the autumn and the winter–spring cohorts of neon flying squid (*Ommastrephes bartramii*) related to the oceanographic regime in the North Pacific: A hypothesis. *Fisheries Oceanography*, **13** (5): 295-309.

Ishida, Y., Azumaya, T., and Fukuwaka, M., 1999. Summer distribution of fishes and squids caught by surface gillnets in the western North Pacific Ocean. *Bulletin of the Hokkaido National Fisheries Research Institute (Japan)*, **0** (63): 1-18.

Meaden, G. J., and Aguilar-Manjarrez, J., 2013. Advances in geographic information systems and remote sensing for fisheries and aquaculture. FAO Eisheries and Aquaculture Technical Paper, No. 552, 1-26.

Mitchell, A., 2005. *The ESRI Guide to GIS Analysis, Volume 2: Spatial Measurements and Statistics*. Esri Press, Redlands, 38-52.

Nishikawa, H., Igarashi, H., Ishikawa, Y., Sakai, M., Kato, Y., Ebina, M., Usui, N., Kamachi, M., and Awaji, T., 2014. Impact of paralarvae and juveniles feeding environment on the neon flying squid (*Ommastrephes bartramii*) winter–spring cohort stock. *Fisheries Oceanography*, **23** (4): 289-303.

Nishikawa, H., Toyoda, T., Masuda, S., Ishikawa, Y., Sasaki, Y., Igarashi, H., Sakai, M., Seito, M., and Awaji, T., 2015. Wind-induced stock variation of the neon flying squid (*Ommastrephes bartramii*) winter–spring cohort in the subtropical North Pacific Ocean. *Fisheries Oceanography*, **24** (3): 229-241.

Oden, N. L., and Sokal, R., 1978. Spatial autocorrelation in biology. 2. Some biological implications and four applications of evolutionary and ecological interest. *Biological Journal of the Linnean Society*, **10**: 229-249.

Pontius, R. G., and Millones, M., 2011. Death to Kappa: Birth of quantity disagreement and allocation disagreement for accuracy assessment. *International Journal of Remote Sensing*, **32** (15): 4407-4429.

Posada, D., and Buckley, T. R., 2004. Model selection and model averaging in phylogenetics: Advantages of Akaike information criterion and Bayesian approaches over likelihood ratio tests. *Systematic Biology*, **53** (5): 793-808.

R Development Core Team, 2014. R: A language and environment for statistical computing. R Foundation for Statistical Computing, Vienna, Austria. 2013, ISBN 3-900051-07-0.

Rodhouse, P., 2001. Managing and forecasting squid fisheries in variable environments. *Fisheries Research*, **54** (1): 3-8.

Tian, S., Chen, Y., Chen, X., Xu, L., and Dai, X., 2010. Impacts of spatial scales of fisheries and environmental data on catch per unit effort standardisation. *Marine and Freshwater Research*, **60** (12): 1273-1284.

Tseng, C.-T., Su, N.-J., Sun, C.-L., Punt, A. E., Yeh, S.-Z., Liu, D.-C., and Su, W.-C., 2013. Spatial and temporal variability of the Pacific saury (*Cololabis saira*) distribution in the northwestern Pacific Ocean. *ICES Journal of Marine Science*, **70** (5): 991-999.

Wang, W., Zhou, C., Shao, Q., and Mulla, D., 2010. Remote sensing of sea surface temperature and chlorophyll-*a*: Implications for squid fisheries in the north-west Pacific Ocean. *International Journal of Remote Sensing*, **31** (17-18): 4515-4530.

Windle, M. J., Rose, G. A., Devillers, R., and Fortin, M.-J., 2009. Exploring spatial non-stationarity of fisheries survey data using geographically weighted regression (GWR): An example from the Northwest Atlantic. *ICES Journal of Marine Science*, **67** (1): 145-154.

Wood, S., 2006. *Generalized Additive Models: An Introduction with R*. CRC Press, Boca Raton, 52-78.

Yan, M., Li, B., and Zhao, X., 2009. Isolation and characterization of collagen from squid (*Ommastrephes bartrami*) skin. *Journal of Ocean University of China*, **8** (2): 191-196.

Yang, M., Chen, X., Feng, Y., and Guan, W., 2013, Spatial variability of small and medium scales, resource abundance of *Ommastrephes bartramii* in Northwest Pacific. *Acta Ecologica Sinica*, **33** (20): 6427-6435.

Yatsu, A., Midorikawa, S., Shimada, T., and Uozumi, Y., 1997. Age and growth of the neon flying squid, *Ommastrephes bartramii*, in the North Pacific Ocean. *Fisheries Research*, **29** (3): 257-270.

Yatsu, A., Watanabe, T., Mori, J., Nagasawa, K., Ishida, Y., Meguro, T., Kamei, Y., and Sakurai, Y., 2000. Interannual variability in stock abundance of the neon flying squid, *Ommastrephes bartramii*, in the North Pacific Ocean during 1979–1998: Impact of driftnet fishing and oceanographic conditions. *Fisheries Oceanography*, **9** (2): 163-170.

Yu, H., Jiao, Y., and Carstensen, L. W., 2013. Performance comparison between spatial interpolation and GLM/GAM in estimating relative abundance indices through a simulation study. *Fisheries Research*, **147**: 186-195.

Yu, W., Chen, X., Chen, Y., Yi, Q., and Zhang, Y., 2015a. Effects of environmental variations on the abundance of western winter-spring cohort of neon flying squid (*Ommastrephes bartramii*) in the Northwest Pacific Ocean. *Acta Oceanologica Sinica*, **34** (8): 43-51.

Yu, W., Chen, X., Yi, Q., and Chen, Y., 2016. Spatio-temporal distributions and habitat hotspots of the winter–spring cohort of neon flying squid *Ommastrephes bartramii* in relation to oceanographic conditions in the Northwest Pacific Ocean. *Fisheries Research*, **175**: 103-115.

Yu, W., Chen, X., Yi, Q., and Tian, S., 2015b. A review of interaction between neon flying squid (*Ommastrephes bartramii*) and oceanographic variability in the North Pacific Ocean. *Journal of Ocean University of China*, **14** (4): 739-748.

(Edited by Qiu Yantao)